Nickel induced crystallization of amorphous silicon thin films

Zhonghe Jin,[a] Gururaj A. Bhat, Milton Yeung, Hoi S. Kwok, and Man Wong[b]
Department of Electrical and Electronic Engineering, The Hong Kong University of Science and Technology, Clear Water Bay, Kowloon, Hong Kong

(Received 26 September 1997; accepted for publication 7 April 1998)

Nickel (Ni) induced crystallization of amorphous silicon (a-Si) has been studied by selective deposition of Ni on a-Si thin films. The a-Si under and near the Ni-covered regions was found to be crystallized after heat treatment at 500 °C from 1 to 90 h. Micro-Auger electron spectroscopy revealed that a large amount of Ni stayed in the region under the original Ni coverage, but no Ni was detected either in the crystallized region next to the Ni coverage or in the amorphous region beyond the front of the laterally crystallized Si. X-ray photoelectron spectroscopy revealed a nonuniform Ni distribution through the depth of the crystallized film under the original Ni coverage. In particular, a Ni concentration peak was found to exist at the interface of the crystallized Si and the buried oxide. It was found that a layer of 5-nm-thick Ni could effectively induce lateral crystallization of over 100 μm of a-Si, but the lateral crystallization rate was found to decrease upon extended heat treatment. Transmission electron microscopy analysis showed that the crystallized film under the Ni coverage was composed of randomly oriented fine grains, while that outside the Ni coverage was mainly composed of large (110)-oriented grains. A unified mechanism is proposed to explain the Ni induced crystallization of a-Si and possible reasons for the reduction in the lateral crystallization rate are discussed. © *1998 American Institute of Physics.* [S0021-8979(98)09713-8]

INTRODUCTION

Metal induced crystallization (MIC) of a-Si, amorphous germanium (a-Ge), or amorphous SiGe has been intensely investigated with either double layers of metal and the amorphous semiconducting material[1–5] or metal implanted into Si[6,7] or Ge.[8] Studies showed that MIC could dramatically decrease the temperature necessary for the crystallization of a-Si and a-Ge. For those metals forming eutectics with Si, it is believed that the dissolution of metal atoms in the a-Si may weaken the Si bonds and enhance the nucleation and growth of crystalline Si.[3] Tan *et al.*[8] further suggested that the breaking of the metastable metal-Si (or -Ge) bonds facilitated the local rearrangement of atoms required for crystallization. On the other hand, for those metals forming silicides with Si, such as Ni, it has been suggested that the formation of silicides with lattice constants close to that of Si is a necessary prerequisite for MIC.[6] Though this seems to indicate epitaxial growth, the exact mechanism needs to be further clarified. Recently, selective deposition of palladium[9] or Ni[10,11] on a-Si thin films was found to induce crystallization of a-Si outside of the metal coverage. This phenomenon has been called metal induced lateral crystallization (MILC).

In this work, both MIC and MILC of a-Si using Ni have been studied using micro-Raman scattering spectroscopy, x-ray photoelectron spectroscopy (XPS), micro-Auger electron spectroscopy (AES), orientation image microscopy (OIM), and transmission electron microscopy (TEM). A unified mechanism is proposed to explain the Ni induced crystallization of a-Si.

EXPERIMENT

Thin 70 nm to 1 μm a-Si films were deposited on oxidized Si wafers by low pressure chemical vapor deposition at 550 °C. SiH_4 was used as the Si source gas at a flow rate of 70 sccm. The deposition pressure was about 300 mTorr. Ni films with thickness ranging from 5 to 10 nm were deposited in an electron beam evaporator at a rate of around 0.02–0.03 nm/s. A quartz resonator was used to monitor the deposition rate and the film thickness. The base pressure in the deposition chamber was 10^{-8} Torr, but rose to 10^{-7} Torr during the evaporation. The wafers were cooled to keep the temperature below 100 °C during the evaporation. Prior to loading the wafers into the evaporator, the native oxide on the a-Si films was removed by dipping the wafers in dilute HF.

Samples with both blanket and patterned Ni coverage were prepared for the study. For patterned Ni samples, a lift-off process using photoresist was employed. The photoresist was first patterned to expose selected regions of the a-Si thin film before the Ni evaporation. After the Ni had been deposited, the wafers were dipped in acetone for over 10 h. Ni deposited on the photoresist was removed together with the photoresist while Ni deposited on the a-Si stayed behind. The wafers were then cut into 1×1 cm^2 square samples for the subsequent heat treatment.

Heat treatment was done at 500 °C in a conventional atmospheric pressure horizontal furnace for duration ranging from 1 to 90 h. During the heat treatment, N_2 was delivered at a flow rate of 5 ℓ/min from a liquid N_2 source (purity above 99.99%) into a 6 in. diameter quartz tube. However, since the tube was not tightly sealed at the loading end, O_2, together with the laboratory air, could diffuse into the tube and degrade the purity of N_2 in the tube.

[a]Current address: Department of Information Science and Electronic Engineering, Zhejiang University, Hangzhou 3100027, China.
[b]Corresponding author; electronic mail: eemwong@ee.ust.hk

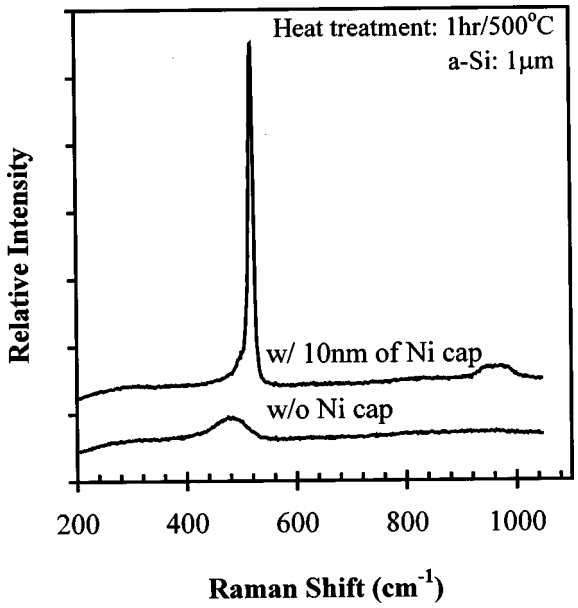

FIG. 1. Raman spectra of the Si films with and without a 10 nm Ni cap after the heat treatment.

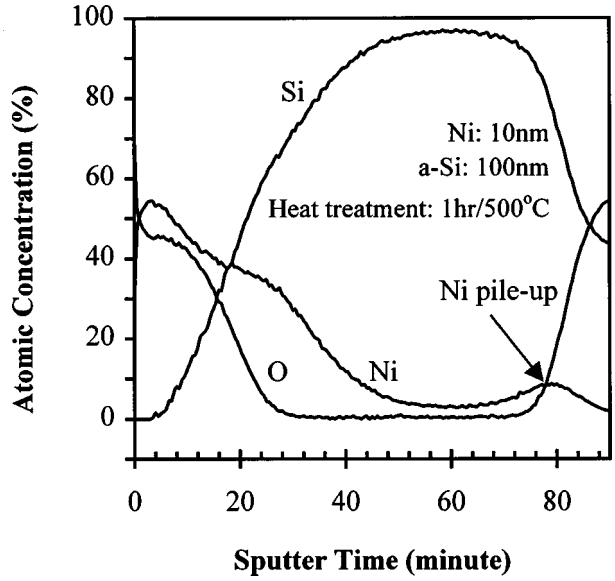

FIG. 2. XPS depth profiles of Si, Ni, and O concentrations in a Ni covered silicon film after 1 h of heat treatment at 500 °C.

Micro-Raman scattering spectroscopy, XPS, AES, OIM, and TEM were used to characterize the samples. A Renishaw 3000 micro-Raman system was used at room temperature with the 514.5 nm line from an Ar ion laser. The backscattered light was collected and focused onto a single grating polychrometer. The dispersed light was detected by a Peltier cooled 576×384 pixel charge coupled device (CCD). The overall resolution was about 2 cm^{-1}. The XPS and AES measurements were carried out in a Perkin Elmer Model PHI 5600 surface analysis system. Ar ions with energy of 4 keV were used for sputtering during depth profiling. The sputter rate was calibrated to be 2 nm/min for thermal silicon dioxide.

RESULTS

The Raman spectra of the samples heat treated with or without a 10 nm Ni cap are shown in Fig. 1. The *a*-Si films were 1 μm thick and heat treated for 1 h at 500 °C. The spectrum of the sample without the Ni cap shows a broad structure near 480 cm^{-1}, with a full width at half maximum (FWHM) of 60 cm^{-1}. This is a broad transverse optical spectrum typically associated with *a*-Si. The spectrum of the sample with the Ni cap has a peak centered at 520 cm^{-1} with FWHM of 8.6 cm^{-1}. The FWHM is larger than the 4.5 cm^{-1} obtained for single crystal silicon, indicating the film is polycrystalline. However, the absence of a broad peak centered at 480 cm^{-1} is apparent, indicating MIC has occurred and the entire film has been crystallized after the heat treatment.

XPS depth profiling was performed on thinner *a*-Si films to further investigate the characteristics of the MIC region. The concentration variations of selected elements across the thickness of a 100 nm *a*-Si film originally capped by 10 nm of Ni are plotted in Fig. 2. The oxygen profile shows a concentration above 40% on the surface, indicating Ni on the surface was partly oxidized. The Ni concentration profile in the crystallized Si film first decreased with Ar sputtering, then stabilized to about 4% in the bulk of the film before finally increasing to about 10% near the interface (indicated by the sharp rise in the XPS oxygen signal) of the film and the buried oxide. Si was not detected on the surface before the Ar sputtering, indicating the diffusion of Si in Ni and NiO_x was slow at the heat treatment temperature of 500 °C.

The changes in the Ni($2p3$), Si($2p3$), and O($1s$) XPS spectra with sputter time are summarized in Fig. 3. The broad Ni($2p3$) peak obtained near the surface—the 1 min line in Fig. 3(a)—indicates that Ni exists as a mixture of NiO, Ni_2O_3, and elemental Ni. Corresponding peaks obtained inside the Si film (the 25, 40, and 75 min lines) are located near a binding energy of 853.6 eV, indicating Ni most likely exists in a silicide-like form. For the Si($2p3$) state, two peaks were detected near 103.5 and 99.7 eV in the subsurface region—the 10 min line in Fig. 3(b)—indicating Si in this region is partially oxidized. This conclusion is further supported by the location of the O($1s$) state—near 533 eV in Fig. 3(c)—obtained at the same depth. The Si($2p3$) peaks in the bulk of the film indicate no significant chemical shifts from the elemental Si value of 99.5 eV.

MILC has been studied using samples with 5 nm of Ni patterned on 70 nm Si thin films. The optical micrograph of a sample heat treated for 16 h at 500 °C is displayed in Fig. 4. Three distinct regions are visible: that with the darkest contrast (area 1) was originally covered by Ni. This is surrounded by a region (area 2) with the brightest contrast, which is in turn embedded in a gray region labeled area 3.

Typical Raman spectra obtained in areas 1, 2, and 3 are presented in Fig. 5. The broad structure near 480 cm^{-1} in the spectrum obtained in area 3 indicates the film remained amorphous. Instead of the broad structure, sharp peaks near 520 cm^{-1} were detected in the spectra obtained in areas 1 and 2, indicating the *a*-Si in these two regions has been crystallized. This provides direct evidence that MIC and MILC have occurred in areas 1 and 2, respectively. The FWHM of the Raman peak obtained in area 2 is about 7.8

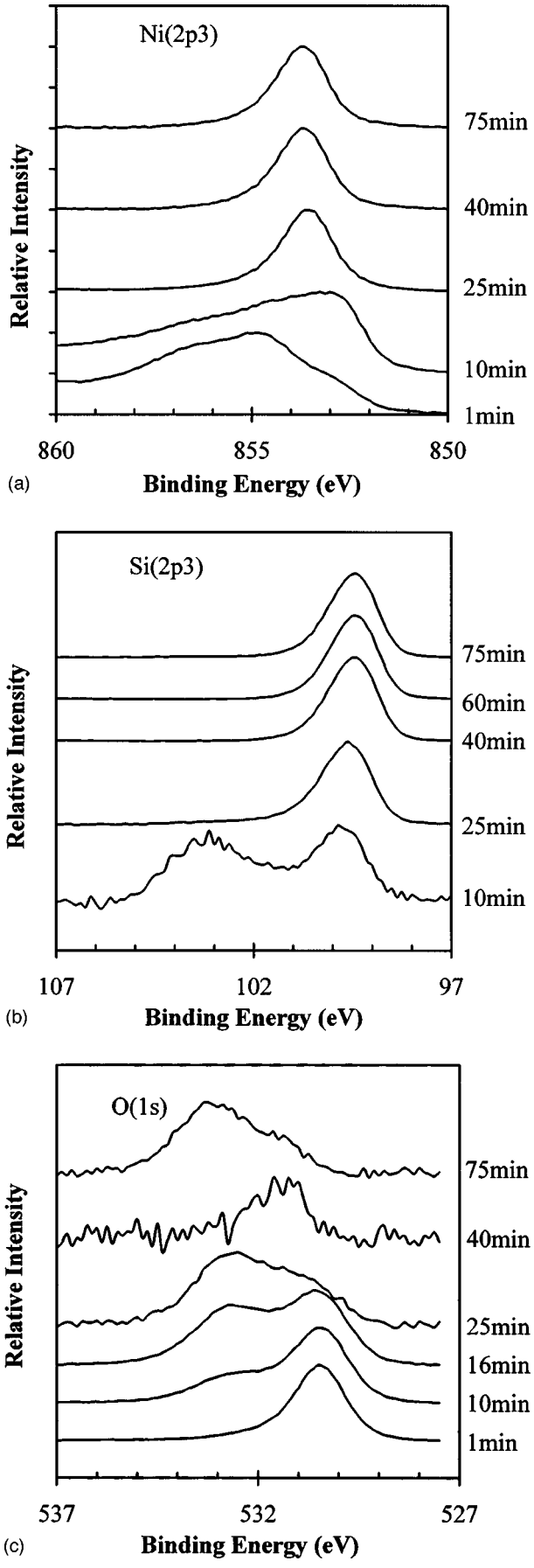

FIG. 3. The variations of the XPS spectra of (a) Ni($2p3$), (b) Si($2p3$), and (c) O($1s$) with sputter time.

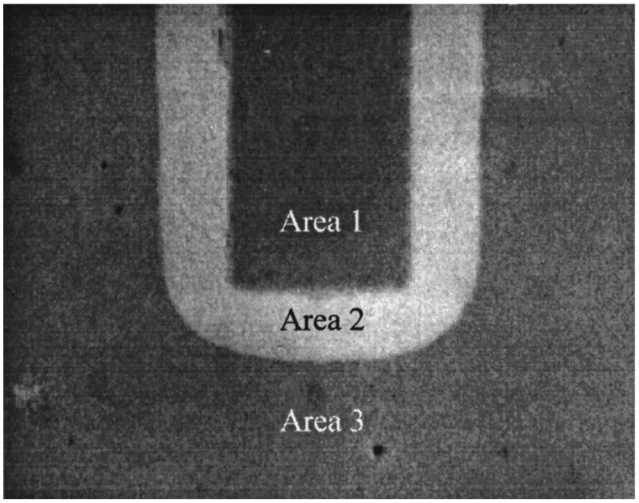

FIG. 4. Optical micrograph of a sample with selectively deposited Ni on a-Si after heat treated for 16 h at 500 °C. The 50-μm-wide Ni lines (area 1) are surrounded by the bright MILC region (area 2). Area 3 is a-Si. The thickness of Ni and Si films are 5 and 70 nm, respectively.

cm^{-1}, smaller than the 8.3 cm^{-1} obtained in area 1, probably indicating the average grain size in the MILC region is larger than that in the MIC region.

TEM and transmission electron diffraction (TED) micrographs taken near the edge of Ni coverage are shown in Fig. 6. Consistent with the Raman results, the dark-field TEM micrograph in Fig. 6(a) shows that the polycrystalline film in the MIC area under the Ni coverage is composed of small grains, while the MILC area outside the Ni coverage is composed of significantly larger grains. The TED micrograph in Fig. 6(b) taken in the MIC area indicates a nearly random distribution of grain orientations, while that in Fig. 6(c) taken

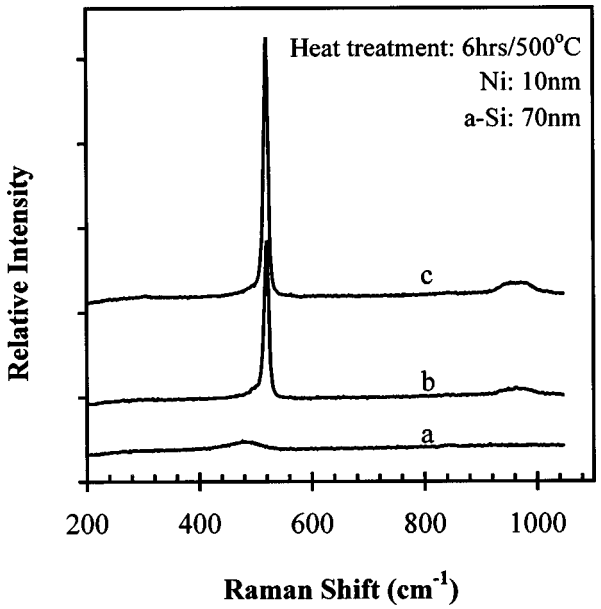

FIG. 5. Typical Raman spectra obtained in (a) the Ni covered region (area 1), (b) the MILC region (area 2), and (c) the amorphous Si region (area 3) in a sample after heat treatment.

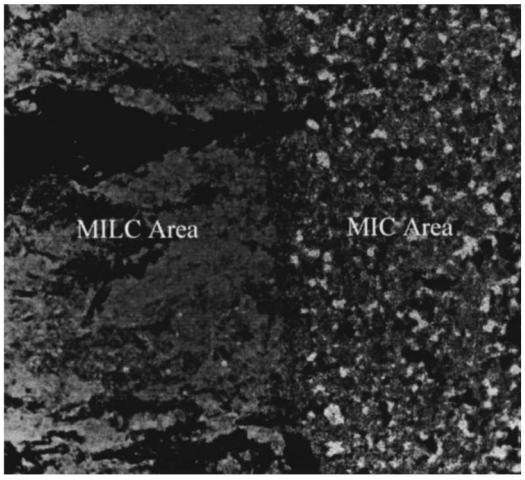

(a)

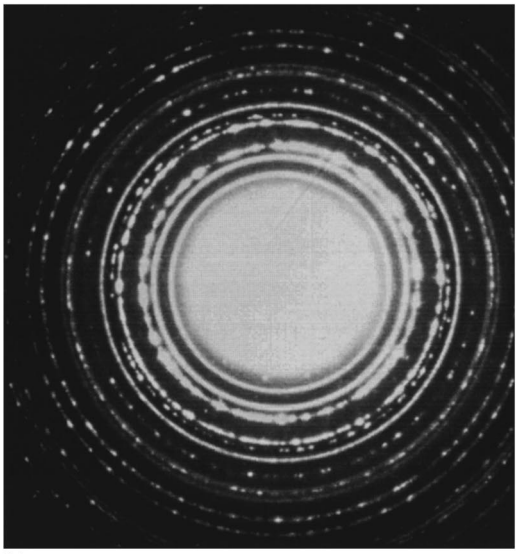

(b)

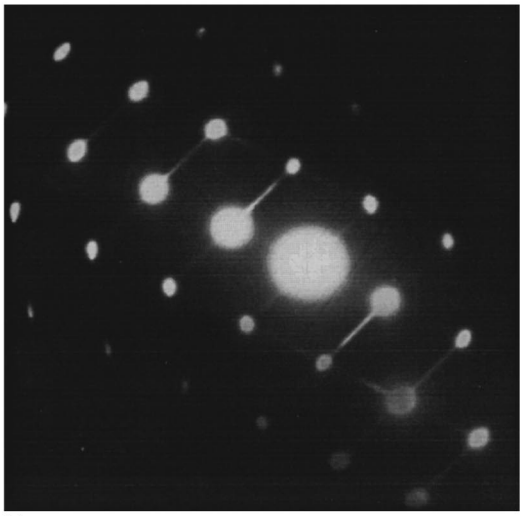

(c)

FIG. 6. TEM and TED micrographs taken in the crystallized silicon film near the edge of the Ni coverage after 16 h of heat treatment at 500 °C. (a) Dark-field TEM micrograph, (b) TED in the MIC area, and (c) TED in the MILC area.

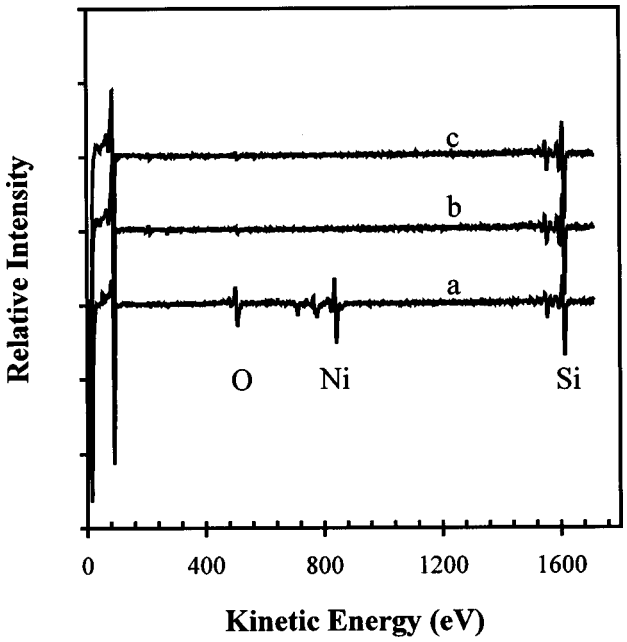

FIG. 7. AES spectra obtained (a) in the MIC region (area 1), (b) in the MILC region (area 2), and (c) in the amorphous Si region (area 3) of a sample with 100 nm amorphous silicon film and 5-nm-thick Ni, after 16 h of heat treatment. The spectra were taken after removing the top surface by a 2 min Ar ion sputtering.

in the MILC area indicates the large grains are primarily (110) oriented.

The gray scale contrast observed in Fig. 4 is probably caused by the different optical coefficients of Ni/NiO_x (area 1), poly-Si (area 2), and *a*-Si (area 3). It is worth noting that the MILC length along the length of the Ni covered lines is similar to that near the end of the Ni line.

The AES spectra obtained in areas 1 (trace a), 2 (trace b), and 3 (trace c) are presented in Fig. 7. The spectra were taken after Ar sputtering of the top surface to remove adsorbed contaminants. Ni signal is significant in area 1, thus indicating a large amount of Ni still remains in the area with the original Ni coverage. The atomic concentrations can be estimated to be 4.64%, 11.63%, and 83.73% for O, Ni, and Si, respectively. Regardless of whether AES was performed before or after the Ar sputtering, no Ni signal was detected either in the MILC region (area 2) or in the amorphous region (area 3), as indicated by the corresponding AES spectra in Fig. 7. Oxygen is detected in both the MILC region and the *a*-Si region even after the Ar sputtering, probably resulting from unintended oxidation during the heat treatment.

After 7 h of heat treatment, it is evident from the OIM micrograph in Fig. 8(a) that the entire area between the Ni covered square islands has been crystallized, with two smooth but wavy crystallization fronts enveloping the islands. The MILC length (L_a) midway along the edge of an island is significantly longer than that (L_b) midway between the islands. After 21 h of heat treatment, the MILC front straightened out, as shown in the OIM micrograph in Fig. 8(b).

The MILC length perpendicular to the long edge of a Ni covered line is plotted as a function of the heat treatment

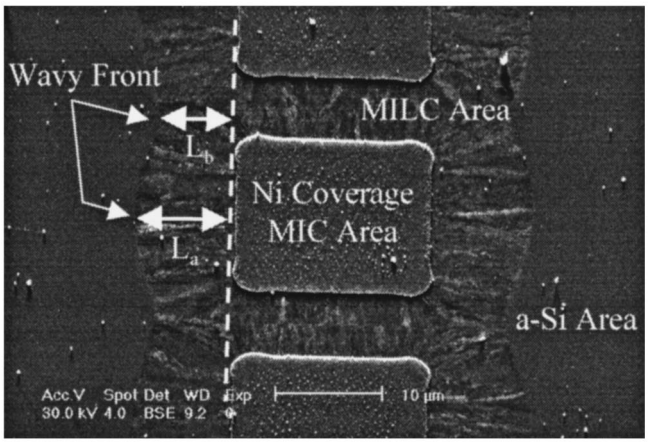

(a)

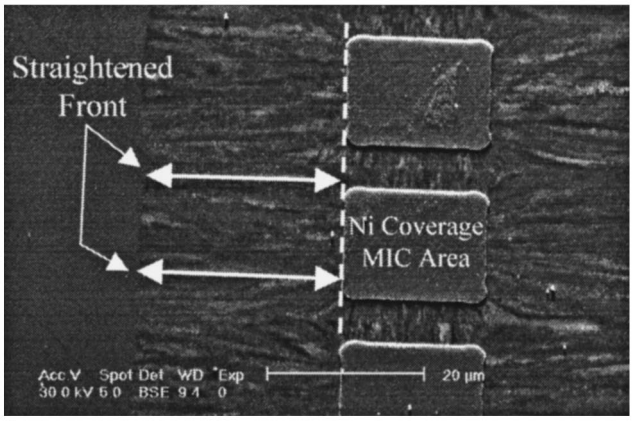

(b)

FIG. 8. OIM micrographs of 100-nm-thick a-Si films with 5 nm of Ni covered square islands after (a) 7 and (b) 21 h of heat treatment at 500 °C.

time in Fig. 9. The measurement was carried out using an optical microscope with a resolution better than 1 μm. The MILC rate as a function of the heat treatment time has been estimated and plotted in Fig. 10. It can be seen that the MILC rate for the 1-μm-thick a-Si sample is slightly higher

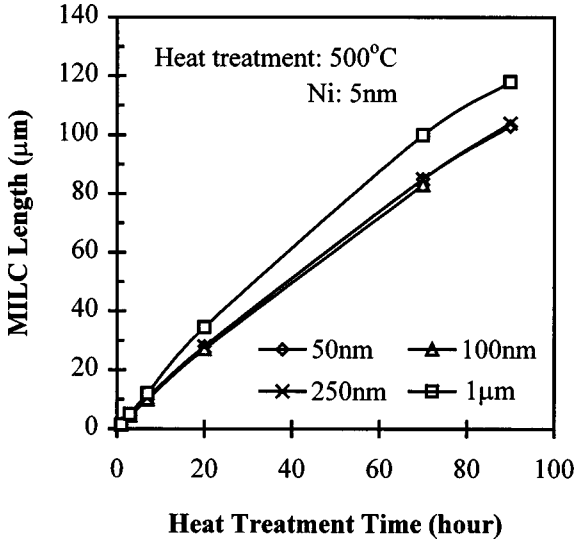

FIG. 9. MILC length as a function of the heat treatment time.

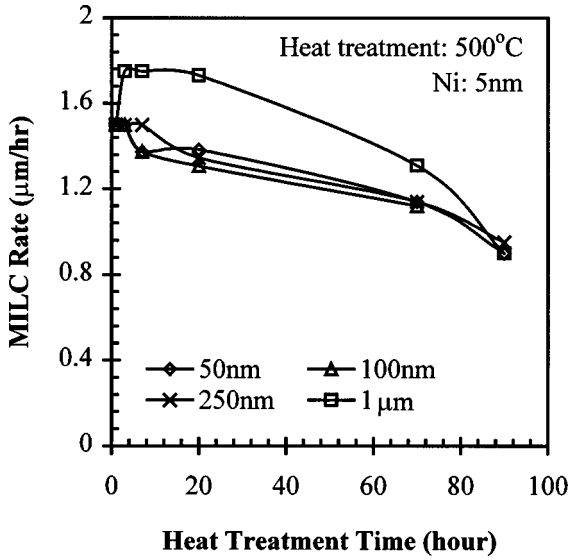

FIG. 10. MILC rate as a function of the heat treatment time.

than those for the other three series of samples with thinner a-Si films. The rate seems to stabilize at 1.7 μm/h for the 1-μm-thick sample between 3 and 20 h of heat treatment. However, the rate clearly decreased upon extended heat treatment for all the samples.

MECHANISM OF MIC AND MILC

The most striking feature resulting from MIC is the appearance of a Ni peak at the bottom of the crystallized film (Fig. 2). Hong *et al.*[12] observed a similar ''inversion''of Ni and Si after silicide induced secondary grain growth of polysilicon. However, they did not suggest any mechanism that could possibly explain the ''long range'' transport of Ni through the entire thickness of the film. This gap in the understanding can be bridged using the observations of Hayzelden *et al.*[13] They proposed that ''nodules''of $NiSi_2$ in an a-Si host first initiated crystallization of Si on some faces of the nodules. Using *in situ* TEM, they observed decomposition of $NiSi_2$ at the interface between the crystallized Si and the $NiSi_2$ nodule and the formation of new $NiSi_2$ at the interface between the nodule and the a-Si. This transportation of Ni through the nodules resulted in the movement of the nodules away from the crystallized regions of Si. Combining the observations of Hong and Hayzelden, we propose that Ni induced MIC of a-Si occurs via a three-step process: silicide formation, breakup of the silicide layer into small nodules, and transport of the silicide nodules through the a-Si film.

At the early stage of the MIC heat treatment, Ni readily reacts with the a-Si[1] and converts itself into $NiSi_2$. Nucleation and growth of small grains of Si crystal than take place randomly along the interface between the $NiSi_2$ and the underlying a-Si. It would not be surprising that the nucleation was aided by the small lattice mismatch between $NiSi_2$ and crystalline Si. Further growth of the crystalline grains eventually leads to the puncturing and break up of the $NiSi_2$ layer. For Ni, Hong[12] reported a low temperature of 500 °C when the plastic deformation accompanying film puncturing oc-

curred. Subsequent to the break up, small nodules of $NiSi_2$ move away from the crystallized top region of the *a*-Si film. Hayzelden[13] observed that nodules with different sizes moved at different speeds, with thinner ones generally moving faster. In the case of MIC, the fastest moving nodules will be found at the crystallization front, which is the interface between the crystallized Si and the *a*-Si. The slower moving nodules will be trapped inside the crystallized region, giving rise to the weak Ni XPS signal detected in the bulk of the film. Once the crystallization front reaches the bottom buried oxide, all remaining moving nodules are stopped, thus contributing to the small peak of Ni XPS signal at the bottom interface of the crystallized silicon thin film in Fig. 2.

Based on the proposed model for MIC, MILC can be easily explained. At the edges of a Ni covered region, a certain number of the break-away $NiSi_2$ nodules will move laterally into the *a*-Si region not originally covered by Ni. As the nodules move laterally, any *a*-Si along the path of the moving nodules will be crystallized. Because the film is thin, crystallization occurs rapidly and any slow moving nodules will be quickly trapped within a short distance from the edges of the Ni covered region, leaving only the fast moving nodules at the MILC crystallization front. This explains why when using TEM, the MILC region was observed to be essentially nodule (hence Ni) free, possibly with only a small number of $NiSi_2$ grains at the crystallization front.[10] Our micro-Auger analysis (spectrum ''*b*'' in Fig. 7) also indicated the MILC region is essentially Ni free. Further evidence of the similarity between MIC and MILC is their comparable rates. The MILC rate of 1.6 μm/h[10,11] at 500 °C is only slightly smaller than the MIC rate of 1.8 μm/h (0.5 nm/s),[13] obtained at a slightly higher temperature of 507 °C.

MILC UPON EXTENDED ANNEALING

The wavy front in Fig. 8(a) can be approximated as the superposition of a sequence of smaller ''circular'' crystallization fronts. These smaller fronts, approximately concentric with the Ni covered square islands, resulted from the two dimensional random isotropic movement of the microscopic $NiSi_2$ nodules in the *a*-Si medium surrounding islands. After a further 14 h of heat treatment, when the radii of the ''circles'' became sufficiently large, the front of each circle flattens out and the waviness disappeared, as shown in Fig. 8(b).

The MILC length as a function of heat treatment time as shown in Fig. 9 clearly shows that the rate of increase of the length slowed down upon extended heat treatment. This trend is obvious from the dependence of the estimated MILC rate on the heat treatment time, as plotted in Fig. 10. A number of factors could be responsible for the reduction in the MILC rate. Since it is known that oxygen contamination could degrade Ni diffusion and its reaction with Si,[14] one possibility is that the residual oxygen in the furnace slowly oxidized the *a*-Si not yet crystallized, thus giving rise to gradually decreasing crystallization rate. But this possibility is eliminated when it is observed that a similar reduction in the MILC rate is present in samples covered by low temperature deposited oxide during the extended heat treatment. Another possibility is that the MILC rate itself would decrease upon extended heat treatment.

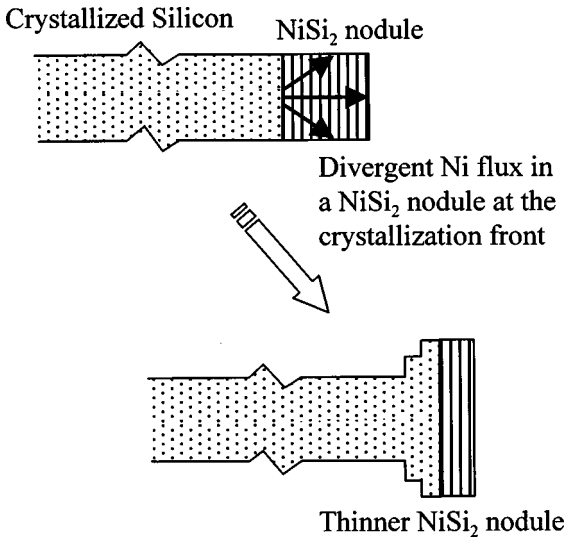

FIG. 11. Schematic drawing showing the ''elongation'' of a $NiSi_2$ nodule during MIC.

Using *in situ* TEM, Hayzelden *et al.*[13] observed an increase in the MIC rate with decreasing size of the $NiSi_2$ nodules and explained the phenomenon in terms of the higher Ni diffusion fluxes through thinner nodules. The projected MIC rate at zero thickness would be infinitely fast. However, this cannot be true in reality since there is no crystallization in the absence of $NiSi_2$ so that the MIC rate must be zero when the thickness is exactly zero. Thus, if the thickness of the nodules are not stable and continue to decrease during the heat treatment, the MILC rate should increase at the beginning, reaches a maximum at a certain critical nodule thickness and subsequently decreases.

Based on Hayzelden's model, which does not impose any restriction on the direction of the Ni diffusion flux as long as it goes from a crystalline interface to an amorphous interface, it is not difficult to understand why the nodules would change shape, becoming thinner along the direction of crystallization and stretching out in the corresponding perpendicular direction. This situation is schematically illustrated in Fig. 11.

SUMMARY

Ni induced crystallization of *a*-Si was studied using micro-Raman, XPS, AES, TEM, and TED analyses. Results show that during MIC, Ni redistributed in the Si film and piled up at the buried interface of the Si film and the oxide substrate. Ni inside the crystallized Si exists in a silicidelike form. A 5-nm-thick patterned Ni can effectively induce crystallization and lateral crystallization of *a*-Si. AES detected no Ni in the MILC region. A unified mechanism is proposed for MIC and MILC and possible reasons for the reduction in the MILC rate during the extended heat treatment are discussed.

ACKNOWLEDGMENTS

The authors gratefully thank Terry Smith and Dr. Lutao Weng for the XPS and AES analyses and helpful discussions, Jason Squire for the Raman analysis, and Dr. Keith Moulding for the TEM/TED analyses. One of the authors (M.W.) would like to acknowledge the helpful discussions with Dr. Fei Deng and Professor S. S. Lau of the University of California at San Diego. This work was supported by a Competitive Earmarked Research Grant from the Research Grants Council of Hong Kong and a grant from the Hong Kong Industry Department.

[1] Y. Kawazu, H. Kudo, S. Onari, and T. Arai, Jpn. J. Appl. Phys., Part 1 **29**, 2698 (1990).
[2] T. J. Konno and R. Sinclair, Mater. Sci. Eng., A **179/180**, 426 (1994).
[3] G. Radnoczi, A. Robertsson, H. T. G. Hentzell, S. F. Fong, and M-A. Hasan, J. Appl. Phys. **69**, 6394 (1991).
[4] B. Mohadjeri, J. Linnros, B. G. Svensson, and M. Ostling, Phys. Rev. Lett. **68**, 1872 (1992).
[5] Z. Jin, G. A. Bhat, M. Yeung, H. S. Kwok, and M. Wong, Jpn. J. Appl. Phys., Part 2 **36**, 1637 (1997).
[6] C. Hayzelden, J. L. Batstone, R. C. Cammarata, Appl. Phys. Lett. **60**, 225 (1992).
[7] A. Yu. Kuznetsow, I. I. Khodos, V. N. Mordkovich, and A. F. Vyatkin, Appl. Surf. Sci. **73**, 253 (1993).
[8] Z. Tan, S. M. Heald, M. Rapposch, C. E. Bouldin, and J. C. Woicik, Phys. Rev. B **46**, 9505 (1992).
[9] S-W. Lee, Y-C. Jeon, and S-K. Joo, Appl. Phys. Lett. **66**, 1671 (1995).
[10] S-W. Lee and S-K. Joo, IEEE Electron Device Lett. **17**, 160 (1996).
[11] S-W. Lee, T-H. Ihn, and S-K. Joo, IEEE Electron Device Lett. **17**, 407 (1996).
[12] Q. Z. Hong, S. Q. Hong, F. M. D'Heurle, and J. M. E. Harper, Thin Solid Films **253**, 479 (1994).
[13] C. Hayzelden and J. L. Batstone, J. Appl. Phys. **73**, 8279 (1993).
[14] P. J. Grunthaner, F. J. Grunthaner, D. M. Scott, M-A. Nicolet, and J. W. Mayer, J. Vac. Sci. Technol. **19**, 641 (1981).